Contrib Mineral Petrol (2014) 167:953
DOI 10.1007/s00410-013-0953-7

ORIGINAL PAPER

Crystallization and eruption ages of Breccia Museo (Campi Flegrei caldera, Italy) plutonic clasts and their relation to the Campanian ignimbrite

Samantha K. Gebauer · Axel K. Schmitt · Lucia Pappalardo · Daniel F. Stockli · Oscar M. Lovera

Received: 23 July 2013 / Accepted: 4 December 2013 / Published online: 17 January 2014

Abstract The Campi Flegrei volcanic district (Naples region, Italy) is a 12-km-wide, restless caldera system that has erupted at least six voluminous ignimbrites during the late Pleistocene, including the >300 km^3 Campanian ignimbrite (CI) which originated from the largest known volcanic event of the Mediterranean region. The Breccia Museo (BM), a petrologically heterogeneous and stratigraphically complex volcanic deposit extending over 200 km^2 in close proximity to Campi Flegrei, has long remained contentious regarding its age and stratigraphic relation to the CI. Here, we present crystallization and eruption ages for BM plutonic ejecta clasts that were determined via uranium decay series and (U–Th)/He dating of zircon, respectively. Despite mineralogical and textural heterogeneity of these syenitic clasts, their U–Th zircon rim crystallization ages are indistinguishable with an average age of 49.7 ± 2.5 ka (2σ errors; mean square of weighted deviates MSWD = 1.2; $n = 34$). A subset of these crystals was used to obtain disequilibrium-corrected (U–Th)/He zircon ages which average 41.7 ± 1.8 ka (probability of fit $P = 0.54$; $n = 15$). This age closely overlaps with published CI $^{40}Ar/^{39}Ar$ eruption ages (40.6 ± 0.1 ka) after recalibration to recently revised flux monitor ages. Concordant eruption ages for BM and CI agree with previous chemostratigraphic and paleomagnetic correlations, suggesting their origin from the same eruption. However, they are at variance with recalibrated $^{40}Ar/^{39}Ar$ ages which have BM postdate CI by 3 ± 1 ka. BM syenites show similar geochemical and Sr–Nd isotopical features of pre-caldera rocks erupted between 58 and 46 ka, but are distinctive from subsequent caldera-forming magmas. Energy-constrained assimilation and fractional crystallization modeling of Nd–Sr isotopic data suggests that pre-caldera magmas formed a carapace of BM-type intrusions in a mid-crust magma chamber (≥8 km depth) shielding the younger CI magma from contamination by Hercynian basement wall rocks. An ~41–50 ka hiatus in crystallization ages implies rapid solidification of these pre-CI intrusions. This argues against protracted pre-eruptive storage of a large volume of CI magma at shallow crustal levels.

Keywords Pleistocene · Tephra · Zircon · Geochronology · (U–Th)/He

Communicated by J. Hoefs.

Electronic supplementary material The online version of this article (doi:10.1007/s00410-013-0953-7) contains supplementary material, which is available to authorized users.

S. K. Gebauer · A. K. Schmitt (✉) · O. M. Lovera
Department of Earth and Space Sciences, University of California, Los Angeles, CA 90095, USA
e-mail: axel@argon.ess.ucla.edu

L. Pappalardo
Sezione di Napoli, Osservatorio Vesuviano, Istituto Nazionale di Geofisica e Vulcanologia, Naples, Italy

D. F. Stockli
Department of Geological Sciences, University of Texas, Austin, TX, USA

Introduction

The Breccia Museo (BM) is a lithic-rich breccia deposit (Campi Flegrei, Naples, Italy) cropping out along the Campi Flegrei caldera border (Fig. 1). It contains abundant fragments of juvenile scorias, hydrothermally altered rocks, and plutonic clasts (e.g., Fedele et al. 2006). Due to the complexity of BM lithology and stratigraphy, its nature

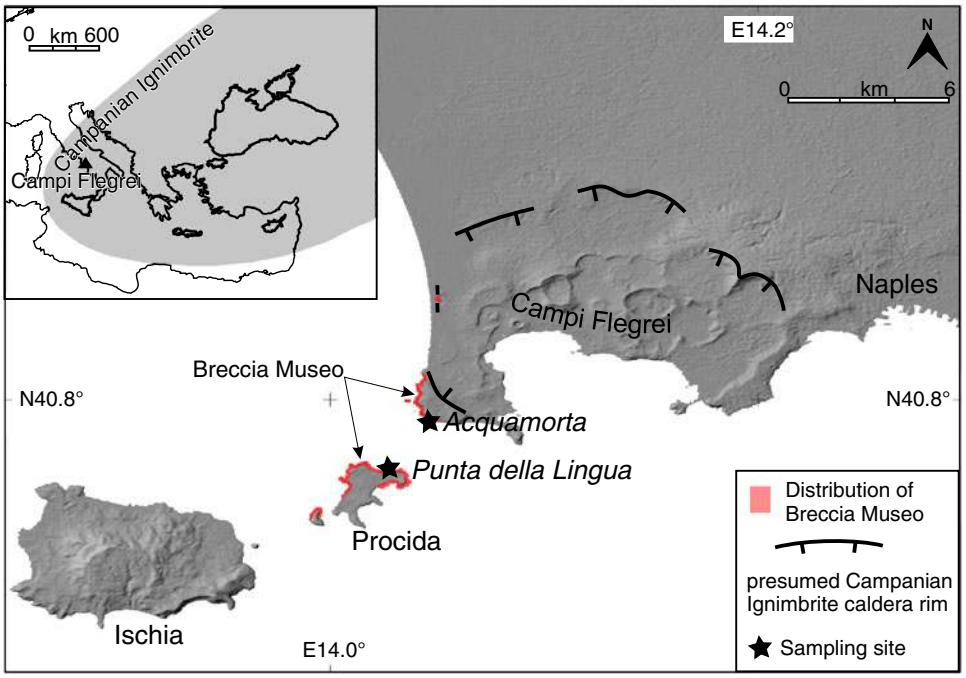

Fig. 1 Map of Campi Flegrei caldera showing extent of Breccia Museo deposits (Fedele et al. 2006) with sampling locations for plutonic clasts. Inset illustrates extent of the Campanian ignimbrite tephra in southeastern Europe within its limits of preservation (corresponding to the 1 cm isopach for unreworked deposits; Fedele et al. 2008a)

has been intensely debated in the literature. Some authors (e.g., Di Girolamo et al. 1984; Melluso et al. 1995; Perrotta and Scarpati 1994) proposed that BM deposits originated from several small eruptions, while others interpreted the BM deposit as the proximal facies of the Campanian Gray Tuff emplaced during the super-eruption of the Campanian ignimbrite (CI) (e.g., Fedele et al. 2008b; Fulignati et al. 2004; Ort et al. 1999; Pappalardo et al. 2002a; Rosi and Sbrana 1987; Rosi et al. 1996). Major questions remain regarding the dissimilar ^{14}C and $^{40}Ar/^{39}Ar$ ages obtained, respectively, from BM (about 21 ka, Lirer et al. 1991) and from CI (about 39 ka, De Vivo et al. 2001; Fedele et al. 2008b), and the relationship between the plutonic clast cargo of the BM eruption and juvenile rocks from the BM and CI.

High spatial and temporal resolution accessory mineral chronology of plutonic rocks erupted in Quaternary volcanoes has greatly contributed to detecting a wide spectrum of processes during pre-eruptive crustal magma accumulation and crystallization. Accessory minerals in plutonic xenoliths often record crystallization within a brief period before eruption, and in some cases, clear evidence exists that volcanic crystals are recycled from largely crystalline rocks (e.g., Bacon and Lowenstern 2005; Bacon et al. 2000, 2007; Lowenstern et al. 2000; Schmitt et al. 2010b). This suggests that plutonic xenoliths are derived from magma chamber margins or coeval intrusions. In other cases, there is little overlap between volcanic and plutonic crystal ages. Zircon crystallization ages in plutonic enclaves from Tarawera volcano (New Zealand), for example, significantly pre-date the age of the volcano as well as the volcanic zircon population (Shane et al. 2012), implying that these much older precursor intrusions remained isolated from subsequent activity. An even more drastic difference between the ages of volcanism and those of associated plutonic rocks was detected in gabbroic enclaves from Redoubt volcano that dating identified as basement xenoliths despite their youthful magmatic appearance conveyed by evidence of partial melting (Bacon et al. 2012).

Here we study a suite of texturally and compositionally heterogeneous plutonic clasts from the BM deposit and apply uranium decay series dating in combination with (U–Th)/He dating of zircon to refine the BM eruption age and to test the hypothesized stratigraphic equivalence of BM and CI. Plutonic clast whole rock and mineral chemical analyses including oxygen and Sr–Nd isotopes were conducted to assess the chemical affinity between BM plutonic rocks and pre-CI magmas. We develop a genetic model where BM plutonic clasts represent a shallow intrusive carapace which was subsequently intruded by the CI caldera-forming magma after a significant amagmatic hiatus. A solidified, albeit still hot intrusive carapace may have aided in shielding the subsequently accumulating CI magma chamber from assimilation of basement wall rocks.

Geological background and sampling

Campanian ignimbrite chronology

The Campania region of southern Italy hosts one of the most historically active volcanic complexes in Europe.

Within this volcanic province, the Campi Flegrei located near Naples (Fig. 1) represents a large cluster of alkaline volcanoes, including the namesake caldera which is the source of the voluminous CI (erupted volume 500 km^3, bulk volume not dense rock equivalent; Fisher et al. 1993). The CI eruption dates to ~40 ka based on $^{40}Ar/^{39}Ar$ sanidine geochronology and caused collapse of a 250 km^2 caldera (Fedele et al. 2008a; Orsi et al. 1996). Ash fallout from this eruption has been found throughout south-eastern Europe from locations within the Tyrrhenian Sea to the Volga River in Russia and the Black Sea (e.g., Lowe et al. 2012; Nowaczyk et al. 2012; Ton-That et al. 2001). Global impact of the CI is inferred from a spike in sulfur abundance observed in Greenland ice cores that coincides with the Laschamp geomagnetic excursion dated at 40.4 ± 2.0 ka (Guillou et al. 2004) and sediment cores from the Black Sea correlated with the Laschamp geomagnetic excursion that contain CI tephra dated at 39.28 ± 0.11 ka (Nowaczyk et al. 2012).

The Breccia Museo (BM) crops out in proximal locations surrounding Campi Flegrei caldera, with its type locality (and thickest sections) in the SW part of the caldera (Fedele et al. 2008b; Perrotta and Scarpati 1994; Rosi et al. 1996). The stratigraphic relations between the BM deposits and the voluminous CI have long been debated because clear contact relations in the field are difficult to establish (Fedele et al. 2008b; Perrotta and Scarpati 1994; Rosi et al. 1996). Moreover, previous geochronology has yielded inconclusive results. ^{14}C ages (Lirer et al. 1991) indicated a significantly younger eruption age for the BM relative to the CI eruption, whereas Ort et al. (1999) and Fedele et al. (2008b) identified the BM and CI due to similar characteristic remanent magnetization orientations and $^{40}Ar/^{39}Ar$ ages, respectively, as proximal and distal correlatives. Chemostratigraphical arguments supporting this correlation are summarized below.

Breccia Museo stratigraphy

The BM is present in isolated outcrops at a maximum thickness of ~50 m along the Campi Flegrei caldera rim, comprising a total volume of ~1.25–2.5 km^3 (Fig. 1; Fedele et al. 2008b). Several detailed accounts of the BM stratigraphy have been presented in the literature (Fedele et al. 2008b; Perrotta and Scarpati 1994; Rosi et al. 1996). Here, we only briefly summarize key aspects that relate to our sampling in the SW part of the Campi Flegrei caldera where BM deposits are best exposed. In some of these locations, the BM directly overlies a paleosoil (Perrotta and Scarpati 1994). A widespread and eponymous unit within the BM is a lithic-rich breccia (breccias unit; BU) which is, in some locations, intercalated with a spatter unit (SU), both attesting to the BM being proximal, although a vent in the Procida Channel remains putative (Fig. 2; Perrotta and Scarpati 1994). The breccia contains petrologically diverse lithic fragments, including country rock, accessory volcanic rocks (often hydrothermally altered), as well as cognate feldspar-dominated cumulate nodules (Fedele et al. 2006, 2008b; Melluso et al. 1995). Perrotta and Scarpati (1994) and Rosi et al. (1996) subdivided the BM into four main stratigraphic units. Later Fedele et al. (2008b) integrated a basal fallout unit. The entire stratigraphic type sequence includes from the base to the top (Fig. 2): a coarse Plinian Pumice Fall (PPF of Fedele et al. 2008b), which is overlain by a unconsolidated, stratified ash unit (USAF of Fedele et al. 2008b) and an ignimbrite deposit, the so-called Piperno formation (WGI of Fedele et al. 2008b, unit A of Rosi et al. 1996); a lithic-rich breccia unit (unit B of Rosi et al. 1996 and LPFU of Perrotta and Scarpati 1994 and of Fedele et al. 2008b); a lithic-rich breccia and spatter agglutinate (unit C of Rosi et al. 1996 and BU/SU of

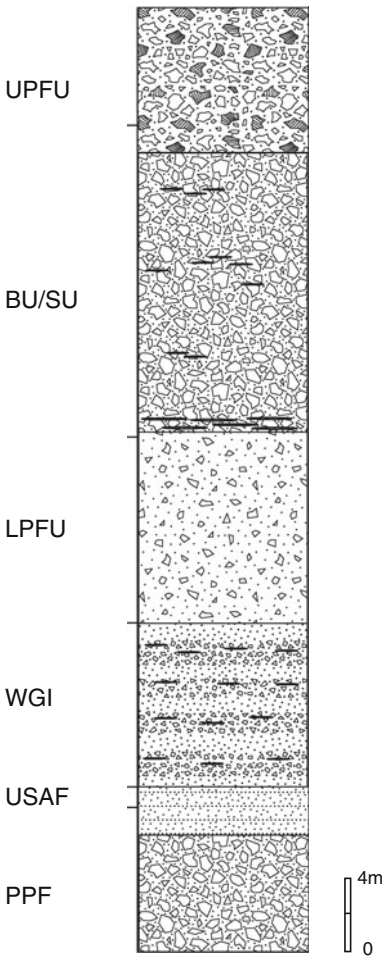

Fig. 2 Schematic stratigraphic column for the BM (Fedele et al. 2008b) and sample number (*right of column*) for clasts collected for study. *UPFU* upper pumice flow unit, *BU* breccia unit, *SU* spatter unit, *LPFU* lower pumice flow unit, *WGI* welded gray ignimbrite, *USAF* unconsolidated, stratified ash, *PPF* Plinian pumice fall

Perrotta and Scarpati 1994 and Fedele et al. 2008b); and an upper low grade ignimbrite (unit D of Rosi et al. 1996 and UPFU of Perrotta and Scarpati 1994 and Fedele et al. 2008b). Rosi et al. (1996), Pappalardo et al. (2002a, b), and Fedele et al. (2008b) have proposed correlations between BM and CI based on the lithologic and geochemical similarities between the proximal BM units and distal CI deposits.

Mineralogy

Six individual clasts of the Breccia Museo from the intermediate lithic-rich breccia unit (the BU of Perrotta and Scarpati 1994 and Fedele et al. 2008b) were selected for this study. For comparison of isotopic data, four juvenile samples (pumice and obsidian) were collected at the same locations and stratigraphic positions. Samples are from two sites: Monte di Procida (Acquamorta 40°47′25.71″N, 14°2′45.52″E, samples: BM S-5-1, S-5-2, BUP, and BUO) and Procida Island (Punta della Lingua 40°45′53.31″N, 14°2′11.10″E, samples BM S-1, S-2, S-3, S-4, PLP, and PLO). These sites are proximal to the caldera and are within 1 and 3 km of its topographic margin, respectively (Fig. 1).

Major phases in plutonic clasts were optically identified and their mode estimated visually. Accessory mineral phases were identified by backscatter electron imaging using a Leo 1430 VP scanning electron microscope (SEM) at UCLA. In addition, energy dispersive X-ray analysis (EDAX) was performed to identify minerals. Subhedral to anhedral potassium feldspar and plagioclase comprise the majority phases of every sample, with abundances of roughly 70 and 20 %, respectively. Cancrinite was identified as a minor component in some samples. Mafic mineral assemblages varied between samples: clinopyroxene is exclusively present in samples BM S-1, BM S-2, and BM S-5-2, whereas only biotite occurs in samples BM S-3, BM S-4, and BM S-5-1, often intergrown with chlorite. Hornblende is often present as an overgrowth over relict clinopyroxene. Accessory minerals are zircon, which is present in all samples, sphene (particularly abundant in BM S-1 and BM S-2), apatite, opaques (abundant in the biotite-bearing nodules BM S-3, BM S-4, and BM S-5-1), and garnet (in BM S-5-1). Zircon is often interstitial, indicating late crystallization (Fig. 3).

Methods

Geochronology

U–Th disequilibrium

Uranium–thorium (U–Th) disequilibrium measurements permit dating of zircon crystallization over timescales of $\sim 10^3$ to 10^5 years, commensurate to the comparatively long half-life of ^{230}Th ($t_{1/2}$ = 75,690 years; Cheng et al. 2000). U–Th zircon ages track crystallization in magmas because U and Th are immobile in zircon even under magmatic conditions (e.g., Cherniak and Watson 2003). In order to concentrate dense accessory minerals for geochronology, the plutonic samples were crushed and sieved to <300 μm. The finest particles were removed from the coarser material in the <300 μm fraction by suspending them in water and carefully decanting them with the supernate liquid. After a final acetone wash, the <300 μm fraction was dried at room temperature. Methylene iodide (MI; nominal density = 3.32 g/cm^3) was used for density separation in a separatory funnel. Zircon (density ~4.6 g/cm^3) and other heavy minerals were collected in coarse filter paper, repeatedly rinsed with acetone to remove MI, and then separated from the magnetic heavy mineral fraction using magnetic separation (hand magnet; Frantz Isodynamic separator). Euhedral, inclusion- and imperfection-free zircons were targeted by hand-picking under a binocular microscope. Approximately 5–15 crystals from each sample were selected. These zircons were pressed into indium metal wells contained within a 2.54-cm-diameter Al mounting disk and coated with a conductive Au layer. Crystal "rim" ages (Fig. 4) were determined by secondary ion mass spectrometry (SIMS) analysis using the UCLA CAMECA ims 1,270 and following analysis protocols in Schmitt et al. (2006). For subsequent (U–Th)/He analysis, crystals were removed from their mounts. Selected crystals that remained in the mount were ground and polished to expose interiors. These crystals were subsequently re-analyzed by SIMS to determine "interior" ages (Fig. 4).

Abundance sensitivity backgrounds resulting from the peak at $^{232}ThO^+$ were subtracted from the $^{230}ThO^+$ peak, as well as the intensities at mass/charge = 244, a proxy for the unresolvable $^{232}Th_2^{12}CO^{2+}$ interference at mass/charge ~246. Background corrections generally amount to <5 % of the ^{230}Th signal. Instrumental mass fractionation resulting from the differential ionization of ThO^+ and UO^+ was corrected by comparing ThO^+/UO^+ to Th/U standard AS3 where the Th/U relative sensitivity was determined from the analysis of $^{208}Pb^+/^{206}Pb^+$. AS3 was also analyzed and interspersed with the BM unknowns; its average $(^{230}Th)/(^{238}U) = 0.999 \pm 0.018$ (MSWD = 0.88; n = 17) agrees with the expected secular equilibrium value of 1.

(U–Th)/He

In contrast to U–Th zircon crystallization ages which typically predate the eruption, (U–Th)/He zircon ages closely track eruptive cooling in volcanic deposits unaffected by subsequent heating (e.g., Schmitt et al. 2010a). To better constrain the BM eruption age, (U–Th)/He zircon analyses

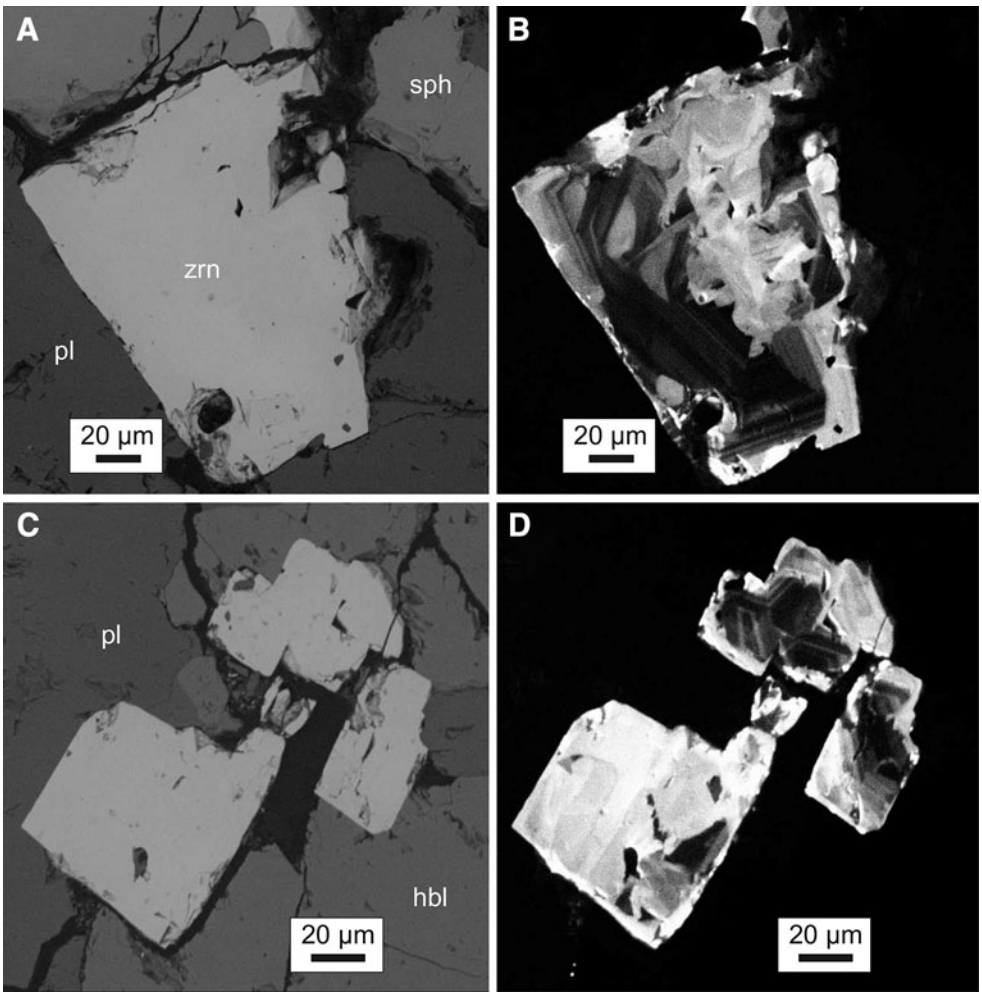

Fig. 3 Scanning electron microscope images of zircon crystals in a thin-section of BM plutonic clast (sample BM S-2). **a** and **c** are backscatter electron (BSE) images; **b** and **c** the corresponding cathodoluminescence (CL) images. Zircon crystals are interstitial to major phases (*pl* plagioclase, *hbl* hornblende) and other accessory minerals (*shp* sphene). Swirly cathodoluminescence domains in some zircon crystals cross-cut oscillatory zonation (**b**), suggesting late-stage dissolution-reprecipitation

were carried out at the University of Kansas using laboratory procedures described in Biswas et al. (2007). Zircons were wrapped in Pt foil, heated for 10 min at 1,290 °C and reheated until >99 % of the He was extracted from the crystal. All ages were calculated using standard α-ejection corrections using morphometric analysis (Farley et al. 1996). After laser heating, zircons were unwrapped from the Pt foil and dissolved using double-step HF-HNO_3 and HCl pressure-vessel digestion procedures (Krogh 1973). U, Th, and Sm concentrations were determined by isotope dilution inductively coupled mass spectrometry (ICP–MS) analysis. The laboratory routinely analyzes zircon standards with independently determined ages, and Fish Canyon tuff zircon analyzed in the same session yielded an age of 28.2 ± 2.3 Ma. Reported age uncertainties reflect the reproducibility of replicate analyses of these laboratory standard samples and estimated analytical uncertainties are ~4 % (1σ) for disequilibrium-uncorrected zircon (U–Th)/He ages.

Because of their young age, U-series disequilibria corrections have a significant impact on (U–Th)/He zircon ages (Farley et al. 2002). The differential partitioning of Th and U results in disequilibrium of the U-series decay series at the time of crystallization, with excesses in ^{230}Th for a crystal/melt partitioning ratio $D_{Th/U} > 1$ and deficits for $D_{Th/U} < 1$. Using reasonable $D_{Th/U}$ (either calculated from whole rock and crystal compositions or from partitioning experimental data), as well as constraints on the crystallization age of the crystal (using the average interior U–Th age), a correction for ^{230}Th deficit or excess can be implemented (Farley et al. 2002; Schmitt et al. 2010a). Similar considerations apply to ^{231}Pa and ^{226}Ra disequilibrium, but these effects are secondary due to the low abundance of the parent and short half-life, respectively.

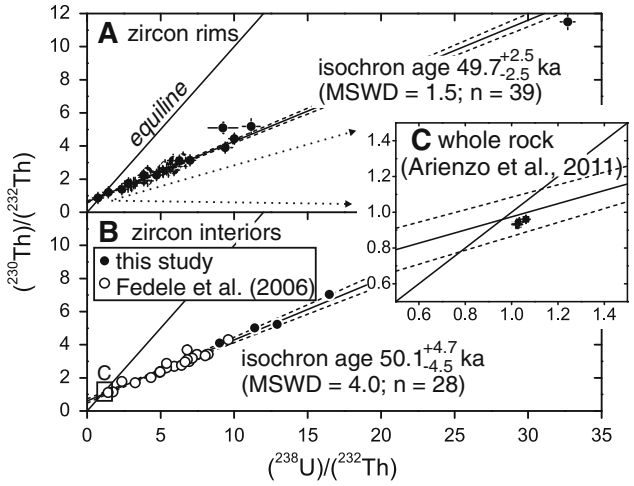

Fig. 4 U–Th isochron diagram for zircon rims (*a*; this study), zircon interiors (*b*; this study and Fedele et al. 2006), and CI glass compositions (*c*; Arienzo et al. 2011)

Crystals zS2-3 and zS2-4 from the same clast serve to illustrate the correction procedures (Table 1; Fig. 5). Their disequilibrium-uncorrected (U–Th)/He ages differ by nearly a factor of two: 28.9 versus 57.7 ka. Both crystals, however, also strongly diverge in their Th/U values: 1.0 versus 12.5. We suspect that the exceptionally high value of zS2-4 (and of several other BM zircons) is due to Th-rich inclusions. Relative to a melt Th/U = 2.94 (using published data for CI Arienzo et al. 2011), zircon zS2-3 crystallized with a lower Th/U than the melt, whereas zS2-4 had higher Th/U than the melt. Initial ^{230}Th was thus depleted in zS2-3 relative to equilibrium, whereas it was enriched in zS2-4. If ^{230}Th deficit persisted in the zircon until the time of eruption, zS2-3 is expected to have experienced delayed accumulation of ^{4}He, whereas ^{4}He accumulation was accelerated in zS2-4. When corrected for these effects, both (U–Th)/He ages converge at 39.5 and 39.6 ka (indistinguishable within uncertainty). This correction assumes uniform disequilibrium at the time of eruption (i.e., the absence of age zonation). This is analogous to assuming a uniform U-distribution for the α-ejection correction as is commonly done in (U–Th)/He dating. We acknowledge that there is ample evidence from natural zircon crystals that both assumptions cannot be universally upheld, and deviations from these general patterns may go unrecognized. This could contribute to a systematic error of (U–Th)/He ages and data scatter. In the case of BM zircons, however, the general validity of assuming uniform ages and concentrations is supported by U–Th zircon rim and interior analyses that yielded closely overlapping ages and U abundances.

Whole rock and isotope geochemistry

Major and trace element analysis

Aliquots of crushed rock from the same plutonic clasts used to extract zircon for geochronology were ground in a corundum shatter-box and analyzed for major and trace elements using established X-ray fluorescence (XRF) and

Table 1 Summary of (U–Th)/He and U–Th geochronology results

Sample	Grain	U (ppm)	Th (ppm)	Sm (ppm)	He (nmol/g)	Mass (μg)	Ft	Equilibrium (U–Th)/He age ± ka	D_{230}	Disequilibrium (U–Th)/He age ± ka
BM S-2	2	2,577	2,626	2.6	0.432	40.7	0.87	28.9 ± 2.3	0.35	39.7 ± 3.4
BM S-2	3	177	2,208	103	0.197	108	0.90	57.7 ± 4.6	4.25	39.6 ± 2.9
BM S-2	5	168	2,182	104	0.198	81.0	0.90	59.8 ± 4.8	4.41	39.9 ± 3.1
BM S-5-2	2	1,002	934	1.2	0.169	58.4	0.88	29.0 ± 2.3	0.32	40.5 ± 3.4
BM S-5-2	3	594	303	0.36	0.0813	74.3	0.90	25.2 ± 2.0	0.20	39.7 ± 3.4
BM S-1	1	1,075	1,139	1.7	0.199	32.7	0.86	31.9 ± 2.6	0.36	42.9 ± 3.7
BM S-1	3	884	283	1.7	0.128	96.6	0.91	27.5 ± 2.2	0.20	43.8 ± 4.0
BM S-1	4	748	214	0.48	0.103	48.5	0.89	27.0 ± 2.2	0.20	42.8 ± 4.0
BM S-1	7	661	510	0.75	0.127	26.0	0.86	35.3 ± 2.8	0.26	53.3 ± 4.3
BM S-1	9	1,039	542	1.0	0.146	47.6	0.88	26.3 ± 2.1	0.20	41.7 ± 3.7
BM S-4	1	1,895	986	1.7	0.252	76.8	0.90	24.5 ± 2.0	0.20	38.3 ± 3.3
BM S-4	2	6,087	23,109	7.4	2.64	32.7	0.86	49.5 ± 4.0	1.29	44.3 ± 3.6
BM S-4	3	3,187	1,992	3.6	0.441	57.7	0.89	25.1 ± 2.0	0.21	38.9 ± 3.4
BM S-4	4	1,869	981	1.5	0.280	47.1	0.89	27.9 ± 2.2	0.20	44.6 ± 4.0
BM S-4	5	1,217	703	1.1	0.191	153	0.92	27.9 ± 2.2	0.20	44.5 ± 4.0

Disequilibrium correction assumes $D_{230} = 0.2$ unless indicated differently due to the presence of Th-rich inclusions, where D_{230} is calculated from zircon Th/U divided by glass Th/U = 2.94 (Arienzo et al. 2011). Disequilibrium is corrected for an average interior crystallization age of 50.1 ± 2.3 ka

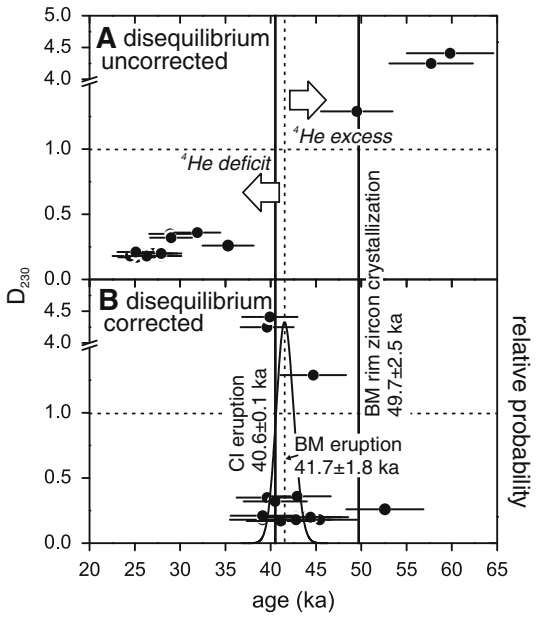

Fig. 5 D_{230} (as a measure of ^{230}Th disequilibrium at the time of crystallization; see text) vs. (U–Th)/He zircon ages prior to disequilibrium correction (*a*), and after disequilibrium correction. Weighted average of disequilibrium-corrected data is shown as a relative probability curve (*right axis*), and represents the BM eruption age which is indicated in comparison with published CI $^{40}Ar/^{39}Ar$ eruptions (De Vivo et al. 2001, recalculated for recent flux monitor recalibrations) and U–Th zircon rim crystallization ages (this study)

ICP analysis protocols at the GFZ Potsdam. Fused disks (Li tetraborate–metaborate) and powders were used for major and trace element determinations, respectively, on a Panalytical Axios XRF spectrometer. Catalytic combustion (Vario EL III) was used to determine H_2O^+ and CO_2. Unless otherwise indicated, we report trace element abundances that were determined by ICP–MS (ELEMENT XR) using diluted HNO_3 solutions following HF, Aqua regia, and $HClO_4$ digestion. For rare earth element (REE) and Y determinations, inductively coupled plasma–atomic emission spectroscopy (ICP–AES) was applied with Na_2O_2 digestion followed by ion-exchange chromatographic extraction of REE + Y (Zuleger and Erzinger 1988). Accuracy was checked through replicate analysis of international reference materials JB-3 and NIM-G.

Radiogenic isotopes

Isotopic analyses for Sr and Nd via thermal ionization mass spectrometry (TIMS) were obtained at the Istituto Nazionale di Geofisica e Vulcanologia—Sezione di Napoli "Osservatorio Vesuviano" (INGV-OV, Naples), using a ThermoFinnigan Triton TI multi-collector mass spectrometer. The samples were exposed to leaching treatment with hot 6 N HCl for 10 min and then washed with pure distilled water ultrasonically. Samples were processed through conventional HF–HNO_3–HCl dissolution before Sr and middle REE (MREE) were separated by standard cation exchange column chemistry, and Nd was further purified on an anion column. Sr and Nd were then loaded onto Ta and Re filaments, respectively. Sr and Nd blanks were negligible for the analyzed samples during the periods of measurements. Measured $^{87}Sr/^{86}Sr$ ratios were normalized for within-run isotopic fractionation to $^{86}Sr/^{88}Sr = 0.1194$, and $^{143}Nd/^{144}Nd$ ratios to $^{146}Nd/^{144}Nd = 0.7219$. The mean measured value of $^{87}Sr/^{86}Sr$ for NIST–SRM 987 was 0.710215 ± 0.000008 (2σ, n = 36) and of $^{143}Nd/^{144}Nd$ for La Jolla was 0.511843 ± 0.000006 (2σ, n = 11). The quoted error is the standard deviation of the mean (2σ) for $n = 180$. Sr and Nd isotope ratios have been normalized to the recommended values of NIST SRM 987 ($^{87}Sr/^{86}Sr = 0.71025$) and La Jolla ($^{143}Nd/^{144}Nd = 0.51185$) standards, respectively.

Stable isotopes

Zircon oxygen isotopes were analyzed by SIMS using multi-collection protocols for the UCLA CAMECA ims1270 described in Trail et al. (2007). Previous geochronology analysis craters were removed by grinding and polishing, and the grain mount was re-coated with a conductive Au layer. Bracketing and interspersed analyses of AS3 zircon ($\delta^{18}O = 5.34$ ‰; Trail et al. 2007) were used to correct for instrumental mass fractionation. Insignificant instrumental drift was noted, and we apply the reproducibility of replicate AS3 analyses of 0.48 ‰ (2σ; $n = 23$) as an estimate for the spot-to-spot uncertainty of the unknowns.

Results

Magma chronology and eruption age

For most samples, a single "rim" spot analysis was conducted per individual zircon crystal, totaling nine rim analyses in BM S-1, four in BM S-2, five in BM S-3, 7 in BM S-4, and ten in BM S-5-2 (Online resource Table 1). Clast BM S-5-1 only yielded two zircon crystals, one of which was analyzed in triplicate. In the $(^{230}Th)/(^{232}Th)$ versus $(^{238}U)/(^{232}Th)$ diagram (Fig. 4), zircon rim analyses generally plot to the right of the equiline, consistent with the expected deficit of ^{230}Th from zircon-melt partitioning behavior (i.e., $D_{Th/U} < 1$). Maximum $(^{238}U)/(^{232}Th)$ is ~32. Because rim analyses are statistically indistinguishable between samples (Online resource Table 1), a free linear regression through all data was used to determine an average crystallization age of 49.7 ± 2.5 ka (2σ uncertainty; mean square of weighted deviates MSWD = 1.49;

$n = 39$). The regression (Fig. 4) encompasses within uncertainty CI glass compositions (Arienzo et al. 2011), suggesting that Th/U estimated from CI glass is a reasonable approximation for the melt composition from which BM zircons crystallized.

Four interior analyses on BM S-1 zircons not used for (U–Th)/He analyses were included with published U–Th zircon interior analyses from Fedele et al. (2006) to calculate an average crystallization age of 50.1 +4.7/−4.5 ka (MSWD = 4.0; $n = 28$). Rim and interior ages are indistinguishable, but a larger dispersion of the interior ages is obvious from the elevated MSWD (Fig. 4). To assess this potential age heterogeneity for the zircon interiors, we also calculated melt-zircon (^{230}Th)/(^{238}U) model ages using CI glasses as the model melt composition (Arienzo et al. 2011). Interior model ages range between 39.4 ± 16.4 and 109 ± 26 ka. Although rim and interior model ages are largely indistinguishable, which indicates rapid zircon crystallization, rare older model ages hint at the presence of antecrystic crystals or crystal domains. Potential source rocks for these antecrysts include pre-CI intrusions related to trachytic eruptions from Campi Flegrei between ~50 and 125 ka (Di Vito et al. 2008).

The zircon crystallization ages are a prerequisite for reliable disequilibrium corrections of the (U–Th)/He ages (Fig. 5). We use an average crystallization age of 50.1 ± 4.6 ka for the crystal interiors because the interior ages represent the bulk volume from which ^{4}He was extracted. In addition, we use $D_{Th/U}$ values from Table 1 to estimate ^{230}Th disequilibrium at the time of crystallization. A minor excess ^{4}He resulting from initial ^{231}Pa excess is corrected by using $D_{Pa/U} = 3$ (Schmitt 2007). The average disequilibrium-corrected (U–Th)/He zircon age is 41.7 ± 1.8 ka (2σ; probability of fit $P = 0.54$; $n = 15$).

Because rapid cooling of the plutonic blocks during ejection and deposition can be reasonably assumed, and the absence of younger deposits overlying the outcrop locations precludes post-depositional reheating and He-loss, this age is interpreted as the BM eruption age. This is also supported by the agreement between ages from two different locations. Sources for systematic age uncertainties include zonation in U and Th abundances as well as internal crystallization age heterogeneity for individual zircon crystals. Minor sources of bias in the disequilibrium-corrected (U–Th)/He zircon ages are disequilibrium inherited from the melt, or ^{226}Ra deficits, but the magnitude of these effects is well within stated uncertainties. U (and Th) abundances vary widely between crystals, but systematic differences between rims and interiors are absent (Online resource Table 1). Although we think that it is very unlikely that all our analyzed zircons had unrecognized old interiors, we explore this effect on the (U–Th)/He age by assuming a uniform 100 ± 10 ka interior age for the disequilibrium correction. Under this assumption, the disequilibrium-corrected average (U–Th)/He age decreases to 36.8 ± 1.9 ka ($n = 15$), but the resulting poor fit ($P = 0.003$) strongly suggests that this is very unlikely.

Magma compositions

The BM clasts show a relatively narrow compositional range from 58.2 to 62.1 wt% SiO_2 and from 1.67 to 5.69 wt% CaO and are mostly classified as syenite in the total alkalis versus silica (TAS) diagram for plutonic igneous rocks (Middlemost 1994; Fig. 6). On major element variation diagrams (Table 2; Fig. 7), the BM syenitic clasts broadly overlap with the trends defined by pre-caldera (dated between 58 and 46 ka; Pabst et al. 2008; Pappalardo et al. 1999) and caldera-forming CI and BM juvenile rocks (Arienzo et al. 2009; Civetta et al. 1997; Fedele et al. 2006; Pappalardo et al. 2002a, b, 2008). CI and pre-CI rocks show negative trends for SiO_2 and Na_2O versus CaO (Fig. 7), whereas total Fe as Fe_2O_3, MgO, K_2O, and P_2O_5 is positively correlated with CaO, and TiO_2 and Al_2O_3 lack systematic trends over the entire CaO range. BM plutonic rocks, however, show more scatter and less systematic (and sometimes opposite) major element variation trends relative to CI and pre-CI volcanic rocks. There are negative correlations between incompatible elements (Nb, Zr, and Y) and Sr, whereas feldspar-compatible Ba and Sr are positively correlated (Fig. 8); additionally, they have similar incompatible trace element ratios (e.g., La/Th and La/Yb; Fig. 9), signifying a potential co-magmatic relation. The BM plutonic clasts generally show more scatter than the volcanic samples, likely due to cumulate

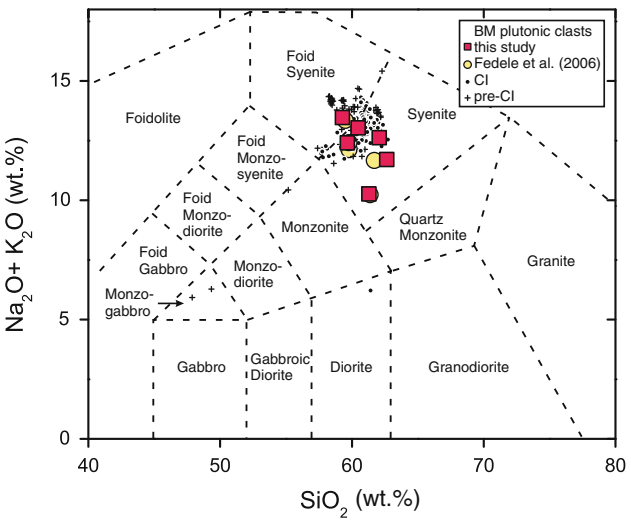

Fig. 6 Total alkali versus silica (TAS) classification diagram for BM plutonic clasts in comparison with CI and pre-CI magma compositions (Arienzo et al. 2009; Civetta et al. 1997; Fedele et al. 2006; Pappalardo et al. 2002, b, 2008)

Table 2 Major and trace element compositions for Breccia Museo plutonic clasts

Sample	BM S-1	BM S-2	BM S-3	BM S-4	BM S-5-1	BM S-5-2
XRF (wt%)						
SiO_2	60.8	60.9	59.2	58.2	59.6	62.1
TiO_2	0.42	0.51	0.54	0.47	0.46	0.42
Al_2O_3	19.1	18.9	18.3	18.0	18.3	19.2
Fe_2O_3	0.99	1.90	6.56	5.58	4.08	1.18
MnO	0.07	0.13	0.20	0.10	0.21	0.07
MgO	0.40	0.98	0.38	0.50	0.58	0.54
CaO	3.75	5.69	1.67	2.02	2.36	3.95
Na_2O	5.19	4.73	3.55	4.17	3.73	4.66
K_2O	7.18	5.47	8.77	9.06	9.12	6.95
P_2O_5	0.06	0.14	0.08	0.08	0.11	0.08
Total	98.0	99.4	99.3	98.2	98.6	99.1
ICP–MS (ppm)						
Li	10	10	17	18	19	11
Be	23	31	8.5	13	8.2	14
Ni	2.5	1.7	3.7	0.88	0.33	0.45
Cu	3.8	2.0	2.2	7.9	3.0	1.2
Rb	280	197	287	364	359	255
Sr	269	353	57	114	194	303
Mo	3.2	2.0	1.1	4.9	3.4	1.1
Cd	76	45	27	83	262	34
Cs	4.8	2.6	2.2	8.2	20	2.7
Tl	941	580	817	1,269	2,100	658
Pb	24	14	23	26	80	20
Bi	52	29	11	58	478	103
Th	25	38	23	26	22	23
U	2.9	5.2	4.6	4.6	5.1	3.2
Sc	2.0	3.2	1.8	1.9	2.4	2.6
Cr	3.7	2.9	7.0	1.7	0.8	1.4
Co	0.5	1.0	4.8	2.1	2.3	0.6
Zn	29	43	139	58	135	24
Ga	20	20	20	19	17	19
Sn	9.0	11	5.1	9.2	4.5	8.3
Sb	0.16	0.10	0.08	0.32	1.09	0.12
XRF (ppm)						
Ba	169	243	41	141	67	195
Nb	98	90	54	77	41	86
Zr	273	366	611	292	246	296
ICP–AES (ppm)						
Y	37	50	23	26	21	35
La	53	99	51	49	54	68
Ce	145	235	92	100	100	155
Pr	18	27	10	12	11	18
Nd	66	96	35	43	38	63
Sm	12	17	6.1	7.9	6.8	11
Eu	1.8	2.4	1.7	1.6	2	1.9
Gd	9.2	13	5.1	6.4	5.5	8.6
Tb	1.5	1.9	0.72	1	0.83	1.3
Dy	7.7	9.9	4.2	5.3	4.2	7
Ho	1.4	1.8	0.95	1	0.77	1.3
Er	3.9	5	2.6	2.8	2.1	3.6
Tm	0.64	0.87	0.41	0.46	0.36	0.6
Yb	3.6	5.1	2.9	2.8	2.1	3.6
Lu	0.49	0.72	0.45	0.38	0.31	0.49
Sc	1.9	2.9	1.5	1.7	2.3	2.5

BM S-1, S-2, S-3 and S-4 from Procida Island (Punta della Lingua 40°45′53.31″N, 14°2′11.10″E)

BM S-5-1 and S-5-2 from Monte di Procida (Acquamorta 40°47′25.71″N, 14°2′45.52″E)

segregation. Deviations from the volcanic trends in Fe_2O_3, MgO, Na_2O, Cr, and V for the syenites are also consistent with biotite and magnetite accumulation, as observed under microscope. Although bulk compositions for BM plutonic clasts are only moderately differentiated, they have high abundances of accessory minerals that are rare in the CI volcanic rocks (e.g., zircon). These accessory minerals thus must have formed late from in situ crystallization of interstitial melt that was more evolved that even the most evolved volcanic compositions, which lack evidence for zircon fractionation (Fig. 3). Trace element spidergrams for BM plutonic clasts also reveal strong enrichments of incompatible trace elements and characteristic depletions for Ba, Sr, P, and Ti that are consistent with fractionation of plagioclase, alkali feldspar, apatite, Fe–Ti oxides, and sphene (Fig. 9).

$^{87}Sr/^{86}Sr$ ratios of BM clasts range from 0.706955 to 0.707898, whereas $^{143}Nd/^{144}Nd$ ratios range from 0.512508 to 0.512526 (Fig. 10; Table 3). BM plutonic clasts plot well within the array of previous data of pre-caldera rocks, while the caldera-forming CI and BM juvenile clasts form a distinct isotopic trend, with lower $^{143}Nd/^{144}Nd$ values and a narrow range of radiogenic Sr (Fig. 10). Because Sr and Nd isotopic ratios of pre-caldera rocks correlate broadly with the degree of differentiation (e.g., correlation coefficient between $^{87}Sr/^{86}Sr$ and Sr $= -0.65$), the potential influence of crustal assimilation in the genesis of these rocks was tested using the energy-constrained assimilation and fractional crystallization (EC-AFC) model of Spera and Bohrson (2001). Crustal rock types characterized by low $^{143}Nd/^{144}Nd$ and high $^{87}Sr/^{86}Sr$ have been evaluated as potential contaminants, with prime candidates being Mesozoic carbonatic rocks and Hercynian crystalline basement recognized by seismic reflection studies between 4 and 8 km depth and $\geq$8 km depth beneath the volcano, respectively (e.g., Berrino et al. 2008; Zollo et al. 2008).

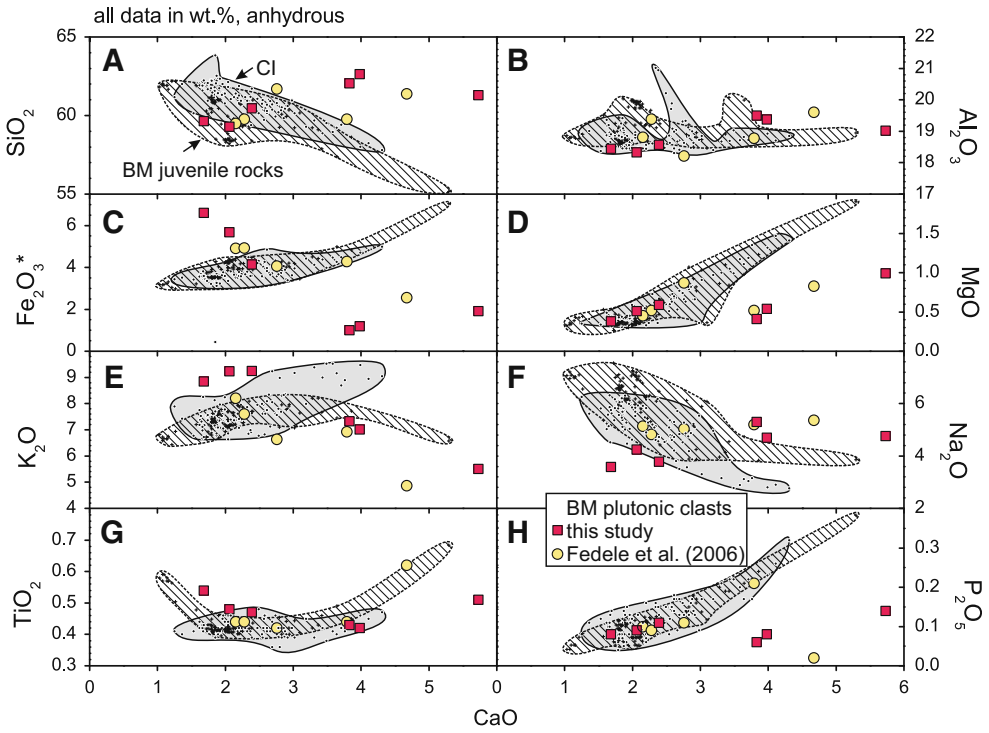

Fig. 7 Major element variation diagrams for BM plutonic clasts (data sources see Fig. 6)

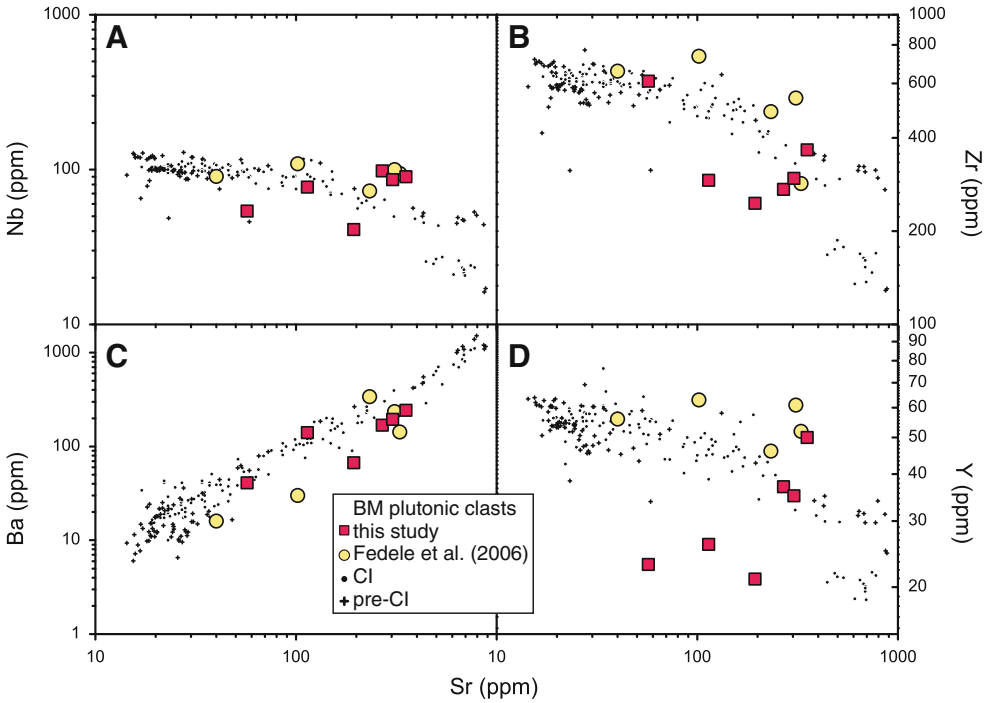

Fig. 8 Trace element variation diagrams for BM plutonic clasts (data sources see Fig. 6)

We considered the intrusion of trachytic magma at a liquidus temperature of 850 °C, calculated by using the MELTS software (Ghiorso and Sack 1995; Asimow and Ghiorso 1998). An ambient crustal temperature of 750 °C (Table 4) was assumed for the intrusion depth, consistent with mid-crustal magma storage and geophysical data suggesting high heat flux in Campi Flegrei area (200 mW/m^2, della Vedova et al. 2001), as well as the high local geothermal gradient (about 150 °C/km) measured in geothermal exploration boreholes inside the caldera (AGIP 1987). The liquidus and solidus temperatures of potential crustal assimilants (Table 4) are based on experimental studies (Wyllie 1977; Lentz 1999; Wolff 1987).

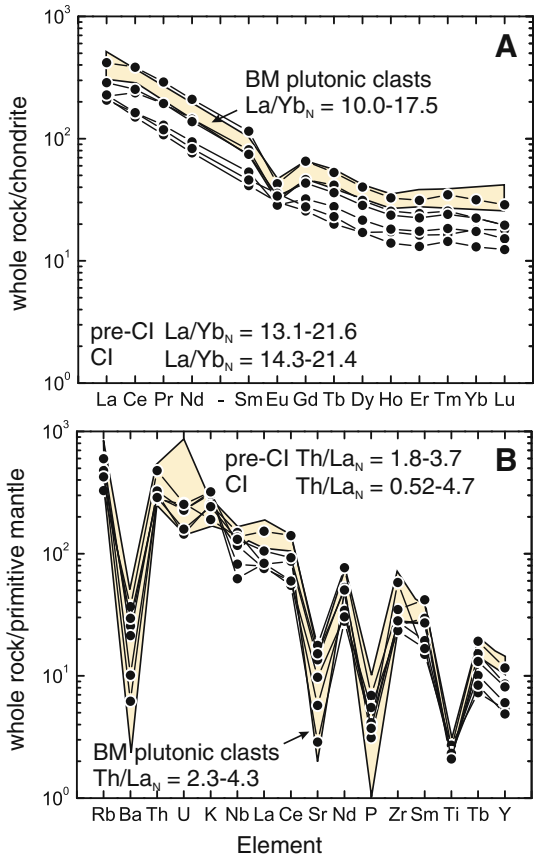

Fig. 9 REE and spidergrams for BM plutonic clasts (data sources see Fig. 6)

EC-AFC models indicate that in a first stage of cooling and crystallization (mass fraction of cumulates = 0.7) at mid-crustal depths, trachyte magma assimilated minor amounts of country rock (mass fraction of anatectic melt = 0.0006) such as Hercynian basement. Assimilation of Hercynian basement, rather than limestone, is probably responsible for the observed Sr and Nd isotopic variations in the BM clasts and juvenile compositions (Fig. 10). Crystalline basement rocks are expected for a reservoir located at ≥8 km depth beneath the volcano where such rocks have been identified on the basis of geophysical data (Berrino et al. 2008; Zollo et al. 2008). This is also supported by melt inclusion studies (Cannatelli et al. 2007; Mangiacapra et al. 2008), high-pressure experiments (Fabbrizio and Carroll 2008), as well as thermodynamic calculations (Fowler et al. 2007; Pappalardo et al. 2008) that indicate the evolution for Campi Flegrei magmas during ascent from a deep (between 400 and 200 MPa) trachybasalt storage zone, toward a shallower (250–150 MPa) trachytic sill (Pappalardo and Mastrolorenzo 2012).

These plutonic rocks are then modeled in a second stage as the intrusive carapace generated during crystallization of pre-caldera magmas. Older syenitic intrusions that form the chamber walls likely have reduced the exchange between younger magma batches and the basement rocks. Our EC-AFC calculations show that the modest Sr–Nd isotopic variations observed in the caldera-forming CI magmas can be reproduced by the assimilation of ~1 % of syenitic carapace for $f = 0.35$. A fractionation mechanism involving sidewall crystallization and liquid fractionation in the magma chamber (Baker and McBirney 1985; Chen and Turner 1980) could explain the high mass of cumulates (65 %) despite the low crystal content observed in most volcanic rocks samples.

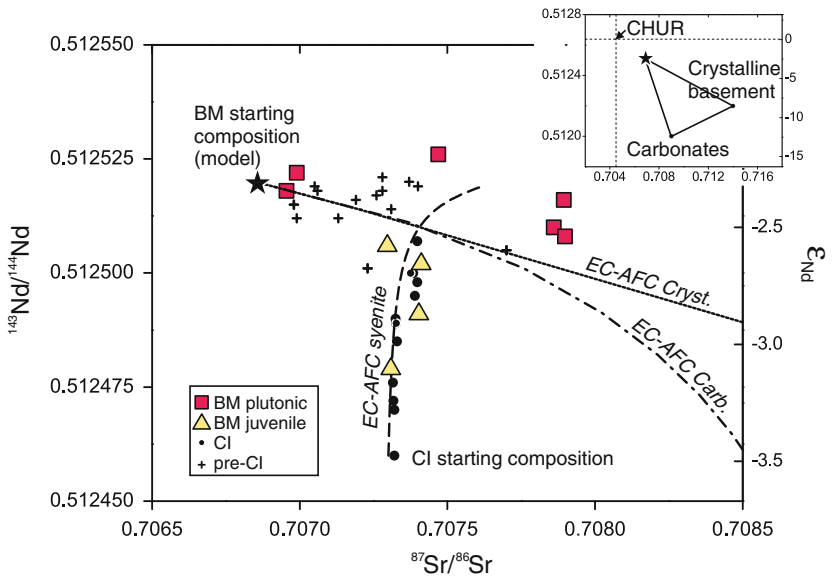

Fig. 10 ^{143}Nd/^{144}Nd versus ^{87}Sr/^{86}Sr compositions and results from energy-constrained assimilation and fractional crystallization (EC–AFC) simulations for BM, pre-CI, and CI rocks (data sources see Fig. 6)

Table 3 Isotopic compositions for Breccia Museo plutonic clasts and juvenile igneous rocks from the same locations

Sample type	BM S-1	BM S-2	BM S-3	BM S-4	BM S-5-1	BM S-5-2	PLO	BUO	PLP	BUP
	Plutonic clasts						Obsidian		Pumice	
$^{87}Sr/^{86}Sr$	0.707894	0.707860	0.706990	0.707469	0.706955	0.707898	0.707298	0.707404	0.707412	0.707311
1 s.e.	0.000006	0.000005	0.000006	0.000006	0.000006	0.000005	0.000006	0.000006	0.000004	0.000040
$^{143}Nd/^{144}Nd$	0.512516	0.512510	0.512522	0.512526	0.512518	0.512508	0.512506	0.512491	0.512502	0.512479
1 s.e.	0.000006	0.000006	0.000008	0.000007	0.000006	0.000006	0.000006	0.000009	0.000006	0.000008
$\delta^{18}O_{SMOW}$ (zircon) ‰	6.10	6.66	6.81	6.16	3.85	6.76	–	–	–	–
1 SD	0.28	0.07	0.24	0.23	1.44	0.23	–	–	–	–
n	3	3	17	3	5	3	–	–	–	–

BM S-1, S-2, S-3, S-4, BUO, and BUP from Procida Island (Punta della Lingua 40°45′53.31″N, 14°2′11.10″E)

BM S-5-1, S-5-2, PLO, and PLP from Monte di Procida (Acquamorta 40°47′25.71″N, 14°2′45.52″E)

SMOW standard mean ocean water ($^{18}O/^{16}O = 0.0020052$)

Table 4 Summary of EC-AFC parameters used for modeling BM, pre-CI, and CI whole-rock isotopic trends

	Pre-caldera		Pre-caldera		Campanian ignimbrite	
Compositional parameters						
Element	Sr	Nd	Sr	Nd	Sr	Nd
Magma conc.	800	40	800	40	700	30
Bulk D_0	3.8	0.16	3.8	0.16	3.8	0.16
Assimilant conc.	350	50	500	10	350	100
Bulk D_0	1.5	0.25	0.7	0.15	3.8	0.25
Isotope	$^{87}Sr/^{86}Sr$	$^{143}Nd/^{144}Nd$	$^{87}Sr/^{86}Sr$	$^{143}Nd/^{144}Nd$	$^{87}Sr/^{86}Sr$	$^{143}Nd/^{144}Nd$
Ratio magma	0.70685	0.51252	0.70685	0.51252	0.7073	0.51246
Ratio assimilant	0.714*	0.512*	0.709**	0.512**	0.7079***	0.51253***

	Hercynian basement	Limestone	Syenitic carapace
Thermal parameters			
Liquidus T magma	850 °C	850 °C	850 °C
Initial T magma	850 °C	850 °C	850 °C
Liquidus T assimilant	1,000 °C	1,000 °C	850 °C
Initial T assimilant	750 °C	750 °C	750 °C
Solidus	800 °C	800 °C	700 °C
Specific heat of magma	1,484 J/kgK	1,484 J/kgK	1,484 J/kgK
Specific heat of assimilant	1370 J/kgK	1370 J/kgK	1370 J/kgK
Enthalpy of cryst. of magma	396,000 J/Kg	396,000 J/Kg	396,000 J/Kg
Enthalpy of melting of ass	270,000 J/kg	270,000 J/kg	270,000 J/kg

In the model melts temperature was calculated using Melts program (e.g. Ghiorso and Sack 1995; Asimow and Ghiorso 1998). An ambient temperature of 750 °C was assigned to crustal rocks consistent with mid-crustal magma storage and geophysical data suggesting a high heat flux under Campi Flegrei. The liquidus and solidus temperature of the different types of crustal rocks has been defined on the basis on experimental studies, between Tla = 1,000 and 800 °C for granodioritic to tonalitic crystalline basement (e.g. Wyllie 1977), between Tla = 1,000 °C and Tsa = 800 °C for limestone (Lentz 1999) and Tla = 850 °C–Tsa = 700 °C for syenite (Wolff 1987). Bulk distributions coefficient for Sr and Nd are from Pappalardo et al. 2008. * Hercynian basement = Rottura et al. 1993. ** Limestone = Iannace 1991. *** Syenite = this study

Zircon oxygen isotopes (Table 3) are a robust indicator for magmatic oxygen compositions because zircon is impervious to post-magmatic alteration or weathering (e.g., Schmitt et al. 2010b). Most samples display zircon $\delta^{18}O$ values between +6.1 ± 0.6 and +6.8 ± 0.6 ‰ (2σ) that overlap with the expected ~2 ‰ (Trail et al. 2009) fractionation between zircon and CI melt (+8.1 ± 0.2 ‰; Taylor et al. 1979). The exception is sample BM S-5-1, which yielded only a few heterogeneous zircon crystals with oxygen isotopic compositions between +5.3 and +1.8 ‰, values characteristic of mantle and low-$\delta^{18}O$ rocks, respectively. These zircons also show comparatively

high (and heterogeneous) U abundances. This indicates that highly evolved melt or fluid that crystallized these zircons became contaminated by a meteoric water component, possibly through assimilation of hydrothermally altered rock.

Discussion

Age of the Breccia Museo eruption relative to the Campanian ignimbrite

Combined U–Th and (U–Th)/He zircon chronology places firm, and mutually consistent, constraints on the BM eruption age as the eruption age must post-date the zircon rim crystallization age of 49.7 ± 2.5 ka. Using the tightly constrained zircon interior crystallization ages (i.e., the average interior crystallization age of 50.1 ka from the U–Th isochron) and U-series disequilibria ($D_{230} \sim 0.2$, and $D_{231} = 3$) at the time of crystallization produces a best estimate for the BM eruption age of 41.7 ± 1.8 ka from (U–Th)/He zircon ages of BM plutonic clasts.

Eruption ages for the BM and CI were previously determined by $^{40}Ar/^{39}Ar$ dating of sanidine (e.g., De Vivo et al. 2001; Fedele et al. 2008b; Rolandi et al. 2003; Ton-That et al. 2001). Because both eruptions coincide with the Laschamp geomagnetic excursion, which may have resulted in presently poorly calibrated shifts in atmospheric ^{14}C (Richards and Andersen 2013), we refrain from a discussion of published ^{14}C ages for BM and CI and instead focus the discussion on available data from $^{40}Ar/^{39}Ar$ geochronology. In the decade since most of the original $^{40}Ar/^{39}Ar$ ages were published, ages of sanidine standards used as irradiation flux monitors in $^{40}Ar/^{39}Ar$ have been scrutinized. Recognizing that this is an ongoing debate (e.g., Renne et al. 2010), we here tentatively discuss recalculated $^{40}Ar/^{39}Ar$ ages (where sufficient detail was presented in the original publication) using one of the more recent recalibrations presented in Rivera et al. (2011). For published $^{40}Ar/^{39}Ar$ ages of BM juvenile rocks (Fedele et al. 2008b), the recalculated eruption age is 37.5 ± 1.1 ka (MSWD = 3.0; $n = 10$) using a Taylor Creek rhyolite flux monitor age of 28.49 Ma (Rivera et al. 2011). Published $^{40}Ar/^{39}Ar$ ages for CI were recalibrated using the same age for Taylor Creek rhyolite as above and an age for Bishop Tuff Quaternary standard of 767.4 ka (Rivera et al. 2011). The resulting CI $^{40}Ar/^{39}Ar$ sanidine ages are 40.6 ± 0.1 ka (MSWD = 4.4; $n = 40$) for multi-grain aliquots from terrestrial deposits (De Vivo et al. 2001) and 40.5 ± 3.5 ka (MSWD = 1.1.; $n = 24$) for marine CI tephra samples (Ton-That et al. 2001). Another constraint for the CI eruption age is from dating of San Martino Upper Tephra, which directly underlies CI within the Naples metropolitan area (Scarpati et al. 2012). Using the same value of Taylor Creek rhyolite as above, we recalculate an age of 40.9 ± 0.6 ka, which constrains a maximum age for the CI eruption.

Published $^{40}Ar/^{39}Ar$ data after recalibration thus display a discrepancy between BM and CI eruption ages, with BM apparently postdating CI by ~3±1 ka. This is at variance with paleomagnetic and chemostratigraphic correlations between proximal and distal units of BM and CI deposits across multiple locations within the Campanian Plain (Fedele et al. 2008b; Ort et al. 1999). We have no explanation for this $^{40}Ar/^{39}Ar$ age discrepancy (even for studies which used the same flux monitor), but disturbance in the K–Ar isotopic system was noted for some BM sanidines by Fedele et al. (2008b). By contrast, our BM (U–Th)/He zircon eruption age agrees within uncertainty with the recalibrated CI $^{40}Ar/^{39}Ar$ sanidine ages. The analytical and systematic age uncertainties of the (U–Th)/He method for young zircons are higher than those frequently reported for $^{40}Ar/^{39}Ar$ chronology, although inter-laboratory bias can considerably exceed stated $^{40}Ar/^{39}Ar$ age uncertainties as illustrated above. The concordance between BM (U–Th)/He and CI $^{40}Ar/^{39}Ar$ ages supported by the geologic evidence implies that the (U–Th)/He method can provide accurate age information for a critical time window between ~ 40 and 50 ka. In this window, ^{14}C dating is particularly vulnerable to analytical and systematic artifacts (e.g., Danisik et al. 2012; Cox et al. 2012), and $^{40}Ar/^{39}Ar$ age accuracy can be compromised, in particular in the absence of datable sanidine or leucite (e.g., Hora et al. 2010).

Crystallization in the pre-campanian magma reservoir

After establishing a close temporal link between the BM and CI eruptions, we investigate how BM plutonic clasts bear upon the understanding of the formation of the CI magma reservoir and its precursors. There is a broad compositional continuity between BM clasts and CI rocks (Figs. 6, 7, 8, 9) which warrant a comparison between crystal ages for both magma systems. We emphasize, however, that there are also small but significant differences in isotopic compositions between BM and CI, which are discussed below. To place zircon crystallization ages into context, we first consider the relative crystallization sequence of BM and CI trachytic magmas. Although zircon saturation in trachytic magmas is not well calibrated (e.g., Boehnke et al. 2013), chemical and textural evidence suggests that zircon crystallized late in the pre-CI magma reservoir (Fig. 3; see also Schmitt 2006; Schmitt et al. 2010b). For BM and CI juvenile rocks, Zr abundance systematically increases with other indicators for melt evolution (e.g., depletion of feldspar-compatible trace

elements such as Sr and Ba; Fig. 8). Zircon textures in BM plutonic clasts (Fig. 3) support late crystallization because crystals are commonly interstitial to the major phases (Fedele et al. 2006; this study). We thus interpret U–Th zircon ages to indicate crystallization in a largely solidified mush. In some cases, low-$\delta^{18}O$, high U/Th, and swirly cathodoluminescence textures (Fig. 3) superimposed onto a magmatic fabric of oscillatory zonation indicate dissolution-reprecipitation of BM zircon crystals by hydrothermal fluids under sub-solidus conditions, but these crystals are indistinguishable in age, and thus, the transition from late magmatic to subsolidus conditions must have occurred very rapidly.

For the six plutonic clasts studied here, all U–Th zircon rim ages overlap. The uniformity of the plutonic U–Th zircon ages is remarkable because the clasts sampled were chaotically deposited in a major explosive event, they are from different sampling locations, and they are compositionally diverse. The ages are also close to new and previously reported zircon interior ages (Fedele et al. 2006). The difference between the average U–Th zircon rim ages (49.7 ± 2.5 ka) and the most precise eruption age (adopting the recalibrated 40.6 ± 0.1 ka $^{40}Ar/^{39}Ar$ sanidine age of De Vivo et al. 2001, and assuming that BM and CI are part of the same eruption) indicates a 9.1 ± 2.5 ka hiatus between crystallization of the pre-CI magma chamber margins and the subsequent evacuation of a large, liquid-dominated magma reservoir, with no evidence for zircon crystallization in between.

U–Th major phase (feldspar, pyroxene, biotite, magnetite, and glass) isochron ages for CI pumice provide further insight into the timescales of magma accumulation prior to the CI eruption. Major mineral isochron ages for the least-evolved CI compositions range between ~45 and 47 ka (Arienzo et al. 2011). These are within error of the zircon rim crystallization ages and thus do not permit a precise resolution of the crystallization sequence. Arienzo et al. (2011) developed a model of recharge of less evolved trachytic magma into a shallow magma reservoir containing evolved trachytic magma which thermally disrupted the crystallization front along the magma chamber margins. Conceivably, the BM intrusions resided at subsolidus conditions for thousands of years and were only disrupted when the CI magma intruded shortly before the eruption.

The uniformity of BM plutonic clast zircon ages contrasts with a more protracted intrusive history recorded by zircon in carbonatite–syenite plutonic xenoliths from the Laacher See magma system (Schmitt 2006; Schmitt et al. 2010b): there, plutonic zircons predate the cataclysmic eruption by up to ~20 ka, but crystallization was quasi-continuous (albeit peaked) until the eruption. The duration of magma accumulation is generally expected to correlate with eruptive volume (e.g., de Saint Blanquat et al. 2011). It therefore seems surprising that BM zircons record a much briefer crystallization interval than Laacher See zircons, despite the CI eruption being >40 times more voluminous than Laacher see (Schmincke et al. 1999). This discrepancy can be resolved if the pre-eruptive thermal, compositional, and physical disruptions affecting the precursor intrusions are more pervasive in a large-volume magma system, compared to a smaller magma body. Rapid assembly of the CI magma body involving high magma recharge fluxes and the associated thermal fluctuations may also explain why observed crystallization ages for zircon (Fedele et al. 2006; this study) and major minerals (Arienzo et al. 2011) are much closer to the eruption age than crystallization durations between ~60 and 300 ka predicted from monotonic magma chamber cooling models (Fowler et al. 2007).

Compositional and isotopic constraints on the origin of the Campanian magma system involving the Breccia Museo plutonic carapace

New geochemical data for BM syenitic clasts in conjunction with published data on pre-CI and CI volcanic samples suggest a complex polybaric magmatic evolution of the Campanian magma system. Particularly, the BM syenitic clasts show strong geochemical and isotopic affinities with respect to the pre-caldera rocks erupted between 58 and 46 ka, whereas they differ from the subsequent caldera-forming magmas. Here, we schematically summarize this magma evolution in multiple stages (Fig. 11). The first stage involves the intrusion of pre-caldera trachytes at a liquidus temperature of 850 °C into the mid-crust at ambient temperature of 750 °C (≥8 km depth). Our EC-AFC models are consistent with an initial phase in which fractional crystallization dominates (horizontal initial path in Fig. 10) while the surrounding Hercynian basement (depth ≥8 km) heats up, followed by contamination when the country rock exceeds its solidus temperature and anatectic melts start to assimilate into the magma body. The studied BM clasts that match the geochemical and isotopic characteristic of pre-caldera rocks (erupted between 58 and 46 ka) represent the cumulates formed at the wall of the mid-crustal (depth ≥8 km) chamber during the AFC process (Fig. 11a). This hypothesis is in agreement with the 49.7 ± 2.5 ka U–Th rim crystallization age of interstitial zircon that represents the age of near-solidus crystallization in this precursor magma body.

In a second stage, subsequent intrusions of fresh CI magma into a mid-crustal reservoir were prevented from reaction with crystalline basement rocks by the presence of a carapace of earlier syenitic intrusions (Fig. 11). These syenitic intrusions were still hot and close to their solidus (Table 4) so that underplating by CI magmas caused

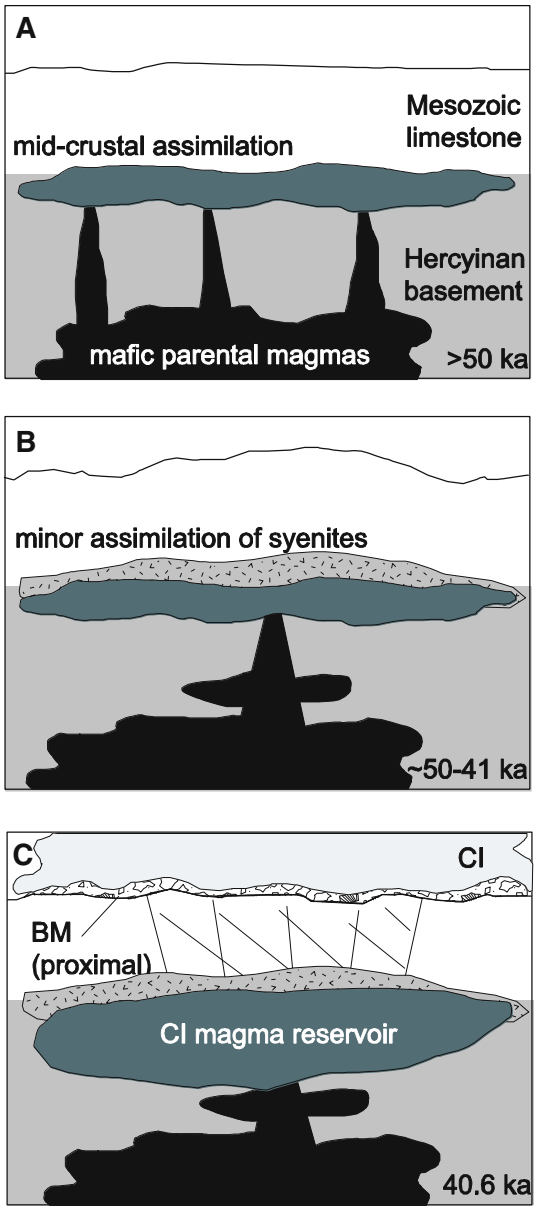

Fig. 11 Simplified scheme illustrating the relationships between BM and CI magma systems (modified after Marianelli et al. 2006). **a** At ~50 ka: intrusion of pre-caldera trachytic magmas (*gray*) into the mid- crust assimilating Hercynian country rocks. The shallow system is fed by a deeper trachybasalt (*black*) magma and heat source; **b** between ~50 and 41 ka: earlier intrusions crystallize and a syenitic carapace (stippled pattern) is formed with the CI magma intruding and assimilating pre-existing syenite intrusions; **c** at 40.6 ka CI magma erupts, disintegrating part of the older syenite intrusions. Synchronous deposition of the Breccia Museo (proximal) and the Campanian ignimbrite (distal) occurs during the caldera-forming eruption

remelting and small degrees of assimilation of these young syenitic wall rocks (Fig. 11b). The caldera-forming magmas filled the reservoir only briefly before the cataclysmic eruption as indicated by major mineral isochron ages that are inconsistent with protracted crystal storage (Arienzo et al. 2011). Violent disruption of the solidified pre-CI intrusions occurred during the initial phases of the CI eruption, leading to the deposition of clast-rich proximal BM deposits (Fig. 11c).

Conclusions

Breccia Museo (U–Th)/He zircon ages (average of 15 single crystal replicates = 41.7 ± 1.8 ka after disequilibrium correction) confirm stratigraphic correlations between BM and CI deposits, whereas age discrepancies of published $^{40}Ar/^{39}Ar$ data preclude such a correlation. Based on this chronologically supported correlation, and recently updated $^{40}Ar/^{39}Ar$ flux monitor ages, we revise the age for the CI/BM eruption to 40.6 ± 0.1 ka. Zircon core-rim U–Th age differences indicate that crystallization in BM plutonic clasts mostly occurred rapidly within a few 1,000 years and that there was a significant hiatus between solidification of BM intrusions and their disintegration during the CI eruption. Isotopic differences between CI and pre-CI magmas can be explained by the formation of chilled reservoir margins that minimized assimilation of basement wall rock by the CI magma. The brief zircon crystallization timescales and the efficiency of shielding of the CI magma imply that pre-CI intrusions cooled rapidly and were solidified by the time the CI magma began to accumulate. This is in support of rapid CI magma accumulation rates and argues against protracted pre-eruptive magma residence at shallow crustal depths.

Acknowledgments The ion microprobe facility at UCLA is partly supported by a grant from the Instrumentation and Facilities Program, Division of Earth Sciences, National Science Foundation. Lucia Civetta is thanked for her precious suggestions during isotope analyses as well as A. Carandente, I. Arienzo, and V. Di Renzo are thanked for technical assistance during samples preparation and Sr–Nd measurements. We thank J. Lowenstern for sharing detailed data of zircon analyses published in Fedele (2006).

References

AGIP (1987) Geologia e geofisica del sistema geotermico dei Campi Flegrei. Tech Rep, SERG-MMESG, San Donato 19

Arienzo I, Civetta L, Heumann A, Wörner G, Orsi G (2009) Isotopic evidence for open system processes within the Campanian ignimbrite (Campi Flegrei-Italy) magma chamber. Bull Volcanol 71(3):285–300

Arienzo I, Neumann A, Wörner G, Civetta L, Orsi G (2011) Processes and timescales of magma evolution prior to the Campanian ignimbrite eruption (Campi Flegrei, Italy). Earth Planet Sci Lett 306(3–4):217–228

Asimow PD, Ghiorso MS (1998) Algorithmic modifications extending MELTS to calculate subsolidus phase relations. Am Mineral 83(9–10):1127–1132

Bacon CR, Lowenstern JB (2005) Late Pleistocene granodiorite source for recycled zircon and phenocrysts in rhyodacite lava at Crater Lake, Oregon. Earth Planet Sci Lett 233(3–4):277–293

Bacon CR, Persing HM, Wooden JL, Ireland TR (2000) Late Pleistocene granodiorite beneath Crater Lake caldera, Oregon, dated by ion microprobe. Geology 28(5):467–470

Bacon CR, Sisson TW, Mazdab FK (2007) Young cumulate complex beneath Veniamin of caldera, Aleutian arc, dated by zircon in erupted plutonic blocks. Geology 35(6):491–494

Bacon CR, Vazquez JA, Wooden JL (2012) Peninsular terrane basement ages recorded by Paleozoic and Paleoproterozoic zircon in gabbro xenoliths and andesite from Redoubt volcano, Alaska. Geol Soc Am Bull 124(1–2):24–34

Baker BH, McBirney AR (1985) Liquid Fractionation 3. Geochemistry of zoned magmas and the compositional effects of liquid fractionation. J Volcanol Geoth Res 24(1–2):55–81

Berrino G, Corrado G, Riccardi U (2008) Sea gravity data in the Gulf of Naples. A contribution to delineating the structural pattern of the Phlegraean Volcanic District. J Volcanol Geoth Res 175(3):241–252

Biswas S, Coutand I, Grujic D, Hager C, Stockli D, Grasemann B (2007) Exhumation and uplift of the Shillong plateau and its influence on the eastern Himalayas: New constraints from apatite and zircon (U–Th-[Sm])/He and apatite fission track analyses. Tectonics 26(6). doi:10.1029/2007TC002125

Boehnke P, Watson EB, Trail D, Harrison TM, Schmitt AK (2013) Zircon saturation re-revisited. Chem Geol 351:324–334

Cannatelli C, Lima A, Bodnar RJ, De Vivo B, Webster JD, Fedele L (2007) Geochemistry of melt inclusions from the Fondo Riccio and Minopoli 1 eruptions at Campi Flegrei (Italy). Chem Geol 237(3–4):418–432

Chen CF, Turner JS (1980) Crystallization in a double-diffusive system. J Geophys Res 85(NB5):2573–2593

Cheng H, Edwards RL, Hoff J, Gallup CD, Richards DA, Asmerom Y (2000) The half-lives of uranium-234 and thorium-230. Chem Geol 169(1–2):17–33

Cherniak DJ, Watson EB (2003) Diffusion in zircon. Rev Mineral Geochem 53(1):113–143

Civetta L, Orsi G, Pappalardo L, Fisher RV, Heiken G, Ort M (1997) Geochemical zoning, mingling, eruptive dynamics and depositional processes—The Campanian ignimbrite, Campi Flegrei caldera, Italy. J Volcanol Geoth Res 75(3–4):183–219

Cox SE, Farley KA, Hemming SR (2012) Insights into the age of the Mono Lake excursion and magmatic crystal residence time from (U–Th)/He and ^{230}Th dating of volcanic allanite. Earth Planet Sci Lett 319:178–184

Danisik M, Shane P, Schmitt AK, Hogg A, Santos GM, Storm S, Evans NJ, Fifield LK, Lindsay JM (2012) Re-anchoring the late Pleistocene tephrochronology of New Zealand based on concordant radiocarbon ages and combined ^{238}U/^{230}Th disequilibrium and (U–Th)/He zircon ages. Earth Planet Sci Lett 349:240–250

de Saint Blanquat M, Horsman E, Habert G, Morgan S, Vanderhaeghe O, Law R, Tikoff B (2011) Multiscale magmatic cyclicity, duration of pluton construction, and the paradoxical relationship between tectonism and plutonism in continental arcs. Tectonophysics 500(1–4):20–33

De Vivo B, Rolandi G, Gans PB, Calvert A, Bohrson WA, Spera FJ, Belkin HE (2001) New constraints on the pyroclastic eruptive history of the Campanian volcanic Plain (Italy). Mineral Petrol 73(1–3):47–65

Della Vedova B, Bellani S, Pellis G, Squarci P (2001) Deep temperatures and surface heat-flow distribution. In: Vai GB, Martini LP (eds) Anatomy of an Orogen, the Apennines and adjacent Mediterranean basins, vol 4. Kluwer Academic Publishers, Dordrecht, p 656

Di Girolamo P, Ghiara MR, Lirer L, Munno R, Rolandi G, Stanzione D (1984) Vulcanologia e Petrologia dei Campi Flegrei. Boll Soc Geol 103:349–413

Di Vito MA, Sulpizio R, Zanchetta G, D'Orazio M (2008) The late Pleistocene pyroclastic deposits of the Campanian Plain: new insights into the explosive activity of Neapolitan volcanoes. J Volcanol Geoth Res 177(1):19–48

Fabbrizio A, Carroll MR (2008) Experimental constraints on the differentiation process and pre-emptive conditions in the magmatic system of Phlegraean Fields (Naples, Italy). J Volcanol Geoth Res 171(1–2):88–102

Farley KA, Wolf RA, Silver LT (1996) The effects of long alpha-stopping distances on (U–Th)/He ages. Geochim Cosmochim Acta 60(21):4223–4229

Farley KA, Kohn BP, Pillans B (2002) The effects of secular disequilibrium on (U–Th)/He systematics and dating of quaternary volcanic zircon and apatite. Earth Planet Sci Lett 201(1):117–125

Fedele L, Tarzia M, Belkin HE, De Vivo B, Lima A, Lowenstern JB (2006) Magmatic-hydrothermal fluid interaction and mineralization in alkali-syenite nodules from the Breccia Museo pyroclastic deposit, Naples, Italy. In: De Vivo B (ed), Volcanism in the Campania Plain—Vesuvius, Campi Flegrei and ignimbrites, 125–161

Fedele FG, Giaccio B, Hajdas I (2008a) Timescales and cultural process at 40,000 BP in the light of the Campanian ignimbrite eruption, Western Eurasia. J Hum Evol 55(5):834–857

Fedele L, Scarpati C, Lanphere M, Melluso L, Morra V, Perrotta A, Ricci G (2008b) The Breccia Museo formation, Campi Flegrei, Southern Italy: geochronology, chemostratigraphy and relationship with the Campanian ignimbrite eruption. Bull Volcanol 70(10):1189–1219

Fisher RV, Orsi G, Ort M, Heiken G (1993) Mobility of a large-volume pyroclastic flow emplacement of the Campanian ignimbrite, Italy. J Volcanol Geotherm Res 56(3):205–220. doi:10.1016/0377-0273(93)90017-L

Fowler SJ, Spera F, Bohrson W, Belkin HE, De Vivo B (2007) Phase equilibria constraints on the chemical and physical evolution of the companion ignimbrite. J Petrol 48(3):459–493

Fulignati P, Marianelli P, Proto M, Sbrana A (2004) Evidences for disruption of a crystallizing front in a magma chamber during caldera collapse: an example from the Breccia Museo unit (Campanian Ignimbrite eruption, Italy). J Volcanol Geoth Res 133(1):141–155

Ghiorso MS, Sack RO (1995) Chemical mass-transfer in magmatic processes. 4. a revised and internally consistent thermodynamic model for the interpolation and extrapolation of liquid-solid equilibria in magmatic systems at elevated-temperatures and pressures. Contrib Miner Petrol 119(2–3):197–212

Guillou H, Singer BS, Laj C, Kissel C, Scaillet S, Jicha BR (2004) On the age of the Laschamp geomagnetic excursion. Earth Planet Sci Lett 227(3–4):331–343

Hora JM, Singer BS, Jicha BR, Beard BL, Johnson CM, de Silva S, Salisbury M (2010) Volcanic biotite-sanidine ^{40}Ar/^{39}Ar age discordances reflect Ar partitioning and pre-eruption closure in biotite. Geology 38(10):923–926

Iannace A (1991) Ambienti deposizionali e processi diagenetici in successioni di piattaforma carbonatica del Trias superiore nei monti Lattari e Picentini (Salerno). Ph.D. thesis. University of Naples, Napoli, pp 216

Krogh TE (1973) Low-contamination method for hydrothermal decomposition of zircon and extraction of U and Pb for isotopic age determinations. Geochim Cosmochim Acta 37(3):485–494

Lentz DR (1999) Carbonatite genesis: a reexamination of the role of intrusion-related pneumatolytic skarn processes in limestone melting. Geology 27(4):335–338

Lirer L, Rolandi G, Rubin M (1991) ^{14}C age of the museum breccia (Campi Flegrei) and its relevance for the origin of the Campanian ignimbrite. J Volcanol Geoth Res 48(1–2):223–227

Lowe J, Barton N, Blockley S, Ramsey CB, Cullen VL, Davies W, Gamble C, Grant K, Hardiman M, Housley R, Lane CS, Lee S, Lewis M, MacLeod A, Menzies M, Muller W, Pollard M, Price C, Roberts AP, Rohling EJ, Satow C, Smith VC, Stringer CB, Tomlinson EL, White D, Albert P, Arienzo I, Barker G, Boric S, Carandente A, Civetta L, Ferrier C, Guadelli JL, Karkanas P, Koumouzelis M, Muller UC, Orsi G, Pross J, Rosi M, Shalamanov-Korobar L, Sirakov N, Tzedakis PC (2012) Volcanic ash layers illuminate the resilience of Neanderthals and early modern humans to natural hazards. Proc Natl Acad Sci USA 109(34):13532–13537

Lowenstern JB, Persing HM, Wooden JL, Lanphere M, Donnelly-Nolan J, Grove TL (2000) U–Th dating of single zircons from young granitoid xenoliths: new tools for understanding volcanic processes. Earth Planet Sci Lett 183(1–2):291–302

Mangiacapra A, Moretti R, Rutherford M, Civetta L, Orsi G, Papale P (2008) The deep magmatic system of the Campi Flegrei caldera (Italy). Geophys Res Lett 35(21):L21304. doi:10.1029/2008GL035550

Marianelli P, Sbrana A, Proto M (2006) Magma chamber of the Campi Flegrei supervolcano at the time of eruption of the Campanian ignimbrite. Geology 34(11):937–940

Melluso L, Morra V, Perrotta A, Scarpati C, Adabbo M (1995) The Eruption of the Breccia Museo (Campi-Flegrei, Italy)—fractional crystallization processes in a shallow, zoned magma chamber and implications for the eruptive dynamics. J Volcanol Geoth Res 68(4):325–339

Middlemost EAK (1994) Naming materials in the magma igneous rock system. Earth Sci Rev 37(3–4):215–224

Nowaczyk NR, Arz HW, Frank U, Kind J, Plessen B (2012) Dynamics of the Laschamp geomagnetic excursion from Black Sea sediments. Earth Planet Sci Lett 351:54–69

Orsi G, De Vita S, di Vito M (1996) The restless, resurgent Campi Flegrei nested caldera (Italy): constraints on its evolution and configuration. J Volcanol Geotherm Res 74:179–214

Ort MH, Rosi M, Anderson CD (1999) Correlation of deposits and vent locations of the proximal Campanian ignimbrite deposits, Campi Flegrei, Italy, based on natural remanent magnetization and anisotropy of magnetic susceptibility characteristics. J Volcanol Geoth Res 91(2–4):167–178

Pabst S, Wörner G, Civetta L, Tesoro R (2008) Magma chamber evolution prior to the Campanian ignimbrite and Neapolitan Yellow Tuff eruptions (Campi Flegrei, Italy). Bull Volcanol 70(8):961–976

Pappalardo L, Mastrolorenzo G (2012) Rapid differentiation in sill-like magma reservoir: a case study from the campi flegrei caldera. Nature's Scientific Reports 2, Article number: 712. doi:10.1038/srep00712

Pappalardo L, Civetta L, D'Antonio M, Deino A, Di Vito M, Orsi G, Carandente A, de Vita S, Isaia R, Piochi M (1999) Chemical and Sr-isotopical evolution of the Phlegraean magmatic system before the Campanian ignimbrite and the Neapolitan Yellow Tuff eruptions. J Volcanol Geoth Res 91(2–4):141–166

Pappalardo L, Civetta L, de Vita S, Di Vito M, Orsi G, Carandente A, Fisher RV (2002a) Timing of magma extraction during the Campanian ignimbrite eruption (Campi Flegrei Caldera). J Volcanol Geoth Res 114(3–4):479–497

Pappalardo L, Piochi M, D'Antonio M, Civetta L, Petrini R (2002b) Evidence for multi-stage magmatic evolution during the past 60 ka at Campi Flegrei (Italy) deduced from Sr, Nd and Pb isotope data. J Petrol 43(8):1415–1434

Pappalardo L, Ottolini L, Mastrolorenzo G (2008) The Campanian ignimbrite (southern Italy) geochemical zoning: insight on the generation of a super-eruption from catastrophic differentiation and fast withdrawal. Contrib Miner Petrol 156(1):1–26

Perrotta A, Scarpati C (1994) The dynamics of the breccia-Museo eruption (Campi-Flegrei, Italy) and the significance of spatter clasts associated with lithic breccias. J Volcanol Geoth Res 59(4):335–355

Renne PR, Mundil R, Balco G, Min KW, Ludwig KR (2010) Joint determination of ^{40}K decay constants and $^{40}Ar^*/^{40}K$ for the fish canyon sanidine standard, and improved accuracy for $^{40}Ar/^{39}Ar$ geochronology. Geochim Cosmochim Acta 74(18):5349–5367

Richards DA, Andersen MB (2013) Time constraints and tie-points in the quaternary period. Elements 9(1):45–51

Rivera TA, Storey M, Zeeden C, Hilgen FJ, Kuiper K (2011) A refined astronomically calibrated $^{40}Ar/^{39}Ar$ age for fish canyon sanidine. Earth Planet Sci Lett 311(3–4):420–426

Rolandi G, Bellucci F, Heizler MT, Belkin HE, De Vivo B (2003) Tectonic controls on the genesis of ignimbrites from the Campanian Volcanic Zone, southern Italy. Mineral Petrol 79(1–2):3–31

Rosi M, Sbrana A (1987) Phlegraean fields, Quaderni de la Ricerca Scientifica 114. CNR, Roma, pp 114–175

Rosi M, Vezzoli L, Aleotti P, De Censi M (1996) Interaction between caldera collapse and eruptive dynamics during Campanian ignimbrite eruption, Phlegrean Fields, Italy. Bull Volcanol 57:541–554

Rottura A, Caggianelli A, Campana R, Delmoro A (1993) Petrogenesis of hercynian peraluminous granites from the Calabrian Arc, Italy. Eur J Mineral 5(4):737–754

Scarpati C, Perrotta A, Lepore S, Calvert A (2012) Eruptive history of Neapolitan volcanoes: constraints from ^{40}Ar–^{39}Ar dating. Geol Mag 150(3):412–425

Schmincke HU, Park C, Harms E (1999) Evolution and environmental impacts of the eruption of Laacher See Volcano (Germany) 12,900 a BP. Quatern Int 61:61–72

Schmitt AK (2006) Laacher see revisited: high-spatial-resolution zircon dating indicates rapid formation of a zoned magma chamber. Geology 34(7):597–600

Schmitt AK (2007) Ion microprobe analysis of $(^{231}Pa)/(^{235}U)$ and an appraisal of protactinium partitioning in igneous zircon. Am Mineral 92(4):691–694

Schmitt AK, Stockli DF, Hausback BP (2006) Eruption and magma crystallization ages of Las Tres Virgenes (Baja California) constrained by combined $^{230}Th/^{238}U$ and (U–Th)/He dating of zircon. J Volcanol Geoth Res 158(3–4):281–295

Schmitt AK, Stockli DF, Niedermann S, Lovera OM, Hausback BP (2010a) Eruption ages of Las Tres Virgenes volcano (Baja California): a tale of two helium isotopes. Quat Geochronol 5(5):503–511

Schmitt AK, Wetzel F, Cooper KM, Zou H, Wörner G (2010b) Magmatic longevity of Laacher see Volcano (Eifel, Germany) indicated by U–Th dating of intrusive carbonatites. J Petrol 51(5):1053–1085

Shane P, Storm S, Schmitt AK, Lindsay JM (2012) Timing and conditions of formation of granitoid clasts erupted in recent pyroclastic deposits from Tarawera Volcano (New Zealand). Lithos 140:1–10

Spera FJ, Bohrson WA (2001) Energy-constrained open-system magmatic processes I: general model and energy-constrained assimilation and fractional crystallization (EC-AFC) formulation. J Petrol 42(5):999–1018

Taylor HP, Giannetti B, Turi B (1979) Oxygen isotope geochemistry of the potassic igneous rocks from the Roccamonfina Volcano, Roman Comagmatic Region, Italy. Earth Planet Sci Lett 46(1):81–106

Ton-That T, Singer B, Paterne M (2001) $^{40}Ar/^{39}Ar$ dating of latest pleistocene (41 ka) marine tephra in the Mediterranean Sea:

implications for global climate records. Earth Planet Sci Lett 184(3–4):645–658

Trail D, Mojzsis SJ, Harrison TM, Schmitt AK, Watson EB, Young ED (2007) Constraints on Hadean zircon protoliths from oxygen isotopes, Ti-thermometry, and rare earth elements. Geochem Geophys Geosyst 8:Q06014. doi:10.1029/2006GC001449

Trail D, Bindeman IN, Watson EB, Schmitt AK (2009) Experimental calibration of oxygen isotope fractionation between quartz and zircon. Geochim Cosmochim Acta 73(23):7110–7126

Wolff JA (1987) Crystallization of nepheline syenite in a Subvolcanic Magma System—Tenerife, Canary-Islands. Lithos 20(3):207–223

Wyllie PJ (1977) Crustal anatexis—experimental review. Tectonophysics 43(1–2):41–71

Zollo A, Maercklin N, Vassallo M, Dello Iacono D, Virieux J, Gasparini P (2008) Seismic reflections reveal a massive melt layer feeding Campi Flegrei caldera. Geophys Res Lett 35(12):L12306. doi:10.1029/2008GL034242

Zuleger E, Erzinger J (1988) Determination of the REE and Y in silicate materials with ICP–AES. Fresen Z Anal Chem 332(2):140–143